Terrestrial LiDAR survey to overcome UAV flight restrictions in morphotectonic analyses: an example from the Budoia–Aviano Thrust (NE Italy)

Fabio Luca Bonali[1,2,*], Lorenzo Suranna[1], Alessandro Luppino[1], Noemi Corti[1], Alberto Villa[1], Giovanni Piccio[1], Sofia Brando[1], Giulia Patricelli[3,4], Enzo Rizzo[4], Maria Eliana Poli[3], and Alessandro Tibaldi[1,2]

[1]Università di Milano Bicocca, Dipartimento di Scienze dell'Ambiente e della Terra, Milan, Italy
[2]Centro Interuniversitario per la Sismotettonica 3D con Applicazioni Territoriali (CRUST), Chieti, Italy
[3]Università di Udine, Dipartimento di Scienze AgroAlimentari, Ambientali e Animali, Udine, Italy
[4]Università di Ferrara, Dipartimento di Fisica e Scienze della Terra, Ferrara, Italy

Corresponding author: fabio.bonali@unimib.it

Introduction

The study area is situated along the outer Pliocene–Quaternary deformation front of the Eastern Southern Alps (ESA) accommodating about 2-3 mm/yr of crustal shortening, as inferred from GNSS-based geodetic observations [Devoti et al., 2011; Serpelloni et al., 2016; Areggi et al., 2023]. This sector is characterised by a belt of curved, WSW–ENE-oriented, SSE-verging thrusts that disrupt Late Pleistocene to Holocene sediments of the Friulian piedmont plain [Galadini et al., 2005; Poli et al., 2021; 2024]. Among these structures, the Polcenigo-Montereale Thrust System comprises multiple SSE verging branches, including the Budoia-Aviano (BA) and Vigonovo (VI) thrusts, both displaying geological and geomorphological indications of ongoing deformation, including pre-LGM conglomerate outcrops, upwarping of the late Pleistocene–Holocene Artugna alluvial fan, drainage anomalies, and morphological scarps (Figure 1) [Poli et al., 2015].

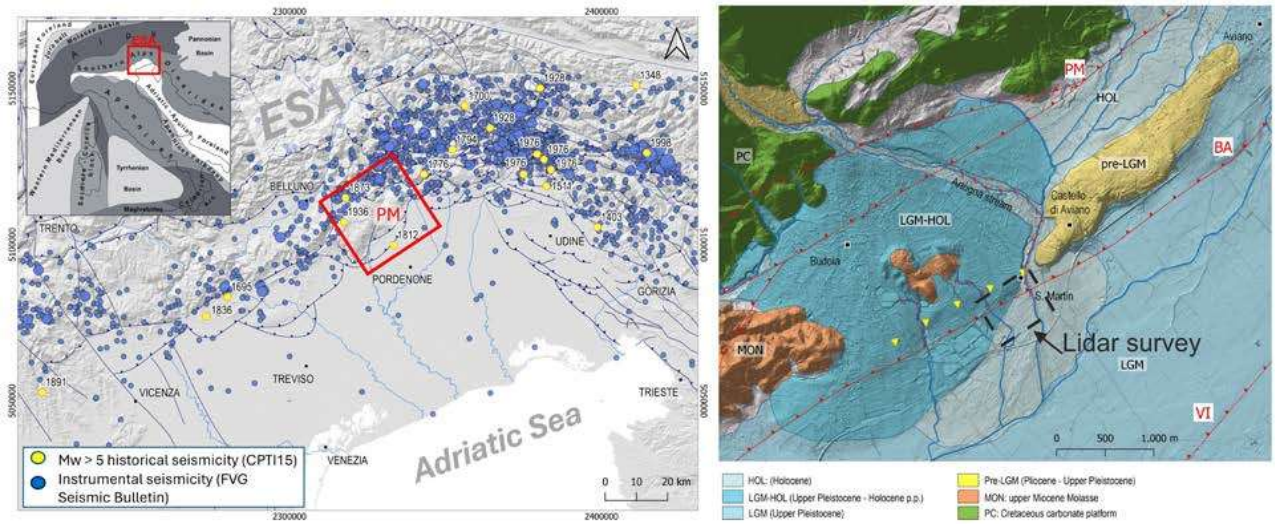

Figure 1 Tectonic and seismic framework of the study area, located at the front of the Carnic Prealpine sector of the Eastern Southern Alps. In the left panel, active faults and instrumental/historical earthquakes [Patricelli et al., 2024; Rovida et al., 2022] are shown. In the right panel, morphotectonic map of the investigated area (modified after Poli et al. [2015]).

Geophysical investigation also highlighted anomalies at depth, possibly related to the recent tectonic activity of the Budoia-Aviano and Vigonovo Thrusts [Rizzo et al., 2024]. In this note, we provide a detailed 3D documentation and analysis of the BA fault zone using a high-resolution, ground-based LiDAR approach. The dataset was acquired with a handheld GeoSLAM ZEB Horizon scanner, enabling the collection of precise morphotectonic information in an area where unmanned aerial vehicle (UAV) operations are prohibited due to the proximity of the Aviano NATO air base (ENAC D-Flight restricted area; Figure 2).

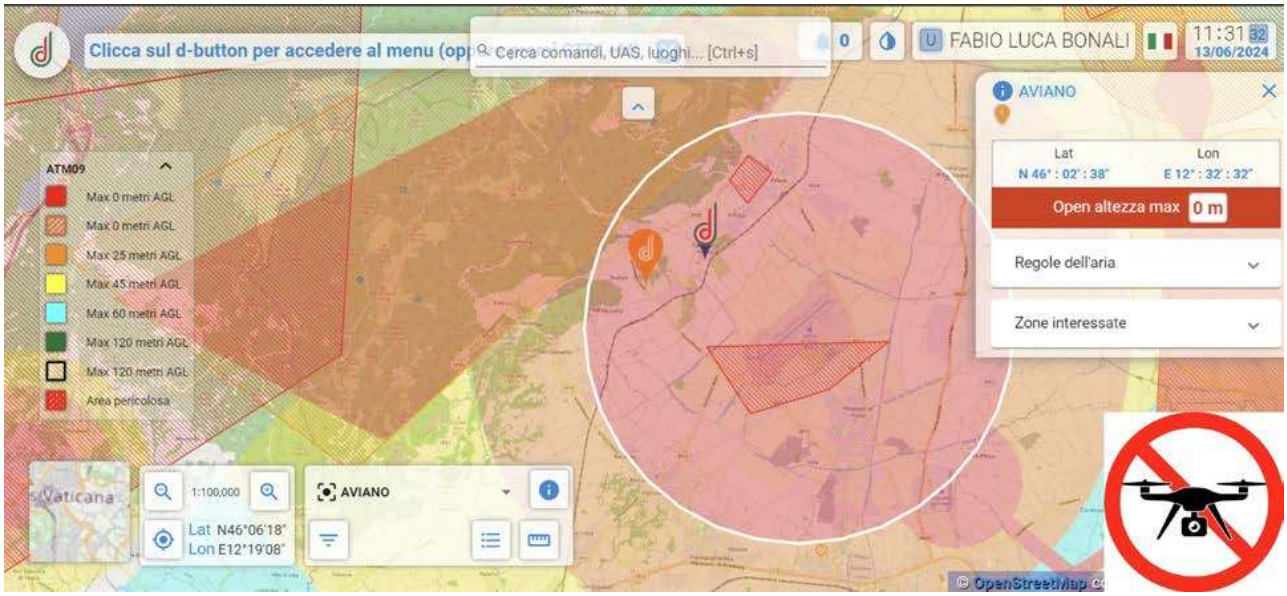

Figure 2 Screenshot from the D-Flight web application [1] showing the airspace restrictions around the Aviano area. The study site (orange marker) lies entirely within the no-fly zone (maximum altitude 0 m AGL) imposed due to the presence of the Aviano NATO air base, which prevents the use of UAVs for photogrammetric surveys. The "drone prohibited" logo was manually added to the image for illustrative purposes.

The results demonstrate that SLAM-based terrestrial LiDAR can achieve spatial resolutions and accuracies comparable to UAV photogrammetry while fully complying with airspace regulations. This approach highlights the potential of portable LiDAR mapping as an effective alternative for studying active fault zones in restricted or logistically challenging environments.

Methodology

Fieldwork was carried out along the BA using a GeoSLAM ZEB Horizon handheld LiDAR coupled with an Emlid Reach RS+ GNSS receiver operating in Real-Time Kinematic (RTK) mode for ground control. To improve efficiency and ensure stable data acquisition, a custom metallic backpack mount was adapted to host the GeoSLAM sensor, its data logging unit, and the RTK antenna (Figure 3). This configuration allowed the operator to perform the survey autonomously even over extended areas, maintaining optimal line-of-sight and positioning stability.

During acquisition, the operator periodically stopped for approximately 10 seconds at selected locations to allow the GeoSLAM system to register fixed reference points, while the same points were simultaneously logged in the GNSS mobile application. The paired measurements

were subsequently employed to achieve absolute georeferencing of the point cloud using the WGS84 reference datum and UTM Zone 33N coordinate system.

Figure 3 Custom backpack-mounted configuration used for the GeoSLAM ZEB Horizon handheld LiDAR survey. The metallic frame was adapted to host the scanner, the data logging unit, and the Emlid Reach RS+ GNSS antenna (operating in RTK mode), allowing autonomous data collection and accurate georeferencing of the point cloud. The system enabled the operator to perform extended surveys efficiently, even across large areas, as shown in the central panel. The right panels show details of the GeoSLAM ZEB Horizon unit and the Emlid Reach RS+ GNSS antenna.

Scanning paths were executed along the main morphotectonic features over an area of roughly 0.4 km². The acquired data were processed using GeoSLAM Connect and GeoSLAM Draw, resulting in a high-resolution Digital Surface Model (DSM) with a spatial resolution of ~2.7 cm/pixel. The integrated LiDAR–RTK workflow achieved a mean RMSE of 0.02–0.03 m, consistent with previously reported performance values [Urban et al., 2024; Petrov et al., 2024]. At the beginning of the acquisition phase, the survey area was subdivided a priori into four smaller sectors, each surveyed individually to optimize data collection and instrument performance. All scanning sessions shared a common network of Ground Control Points (GCPs) acquired in RTK mode, ensuring precise alignment among the different datasets. This strategy allowed effective management of acquisition time and data size while maintaining consistent georeferencing accuracy.
The four point clouds (Figure 4) were referenced and merged in GeoSLAM Connect, producing a single unified point cloud for the area of interest. This dataset was then imported into Agisoft Metashape, where it was processed to generate the final high-resolution Digital Surface Model (DSM) used for subsequent morphotectonic analysis, with a final resolution of 2.7 cm/pixel.

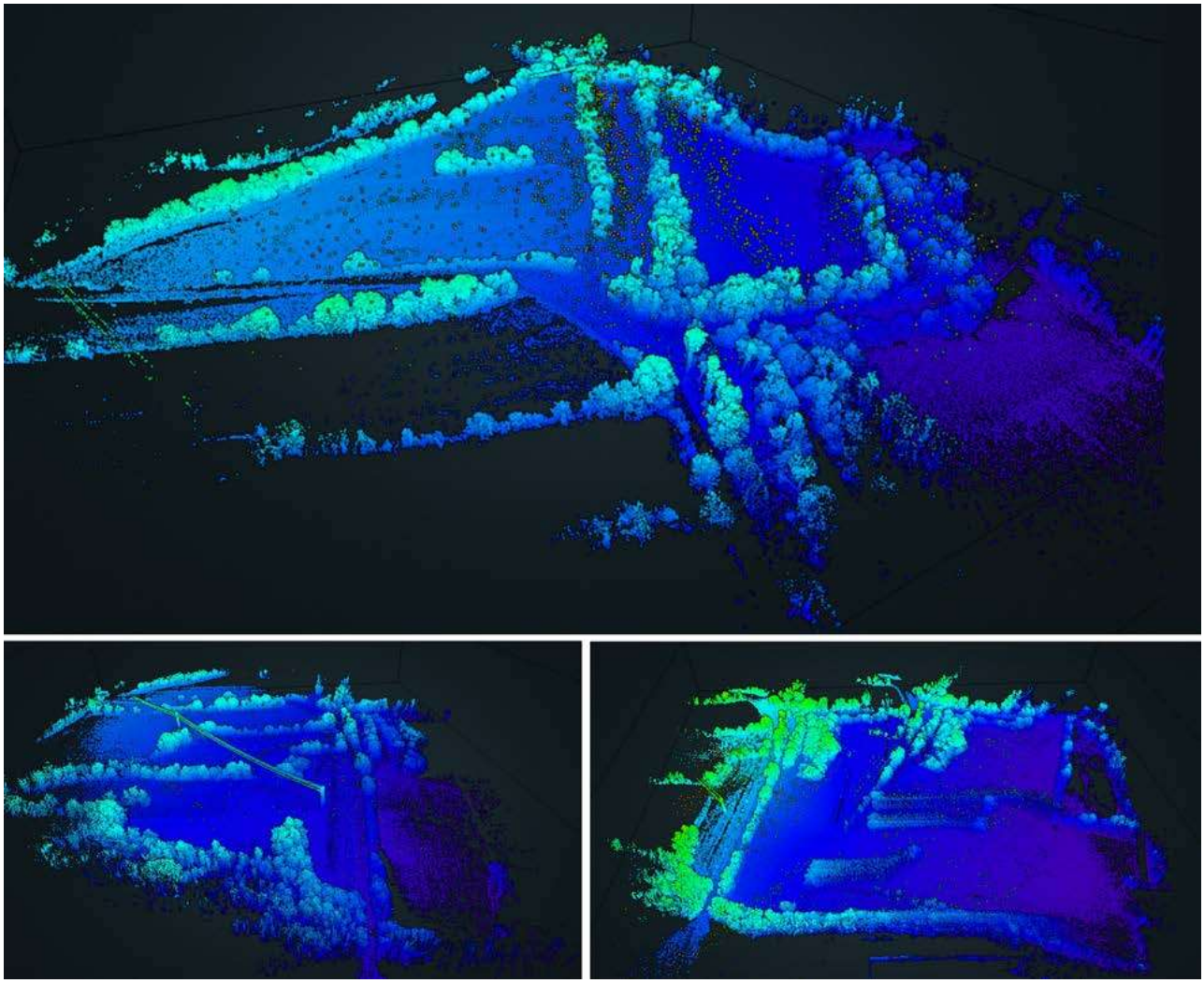

Figure 4 Preliminary results of the GeoSLAM survey showing three of the four independently acquired point clouds corresponding to the subdivided survey areas along the Budoia-Aviano Thrust. Each coloured cloud (blue-green-purple scale) represents one of the scanned sectors, illustrating differences in elevation. These datasets were later merged and processed to generate the high-resolution DSM.

Results and applications

The first outcome of the survey was the generation of a single, unified point cloud (Figure 5), produced in GeoSLAM Connect by merging the four individual scans acquired in the field. This was made possible by the use of a common network of RTK Ground Control Points (GCPs), which ensured precise spatial consistency among the datasets. The automatic alignment provided by GeoSLAM Connect significantly reduced the need for manual post-processing, resulting in a seamless 3D representation of the surveyed area.

This unified point cloud forms the basis for all subsequent analyses, including the production of the high-resolution Digital Surface Model (DSM) in Agisoft Metashape (Figure 6) and the identification of morphological features that deserve further studies to understand if they are associated with the Budoia–Aviano Thrust.

Moreover, the newly generated DSM can also be used as a reference dataset to extract accurate X, Y, Z information for the integration of Ground Penetrating Radar, seismic, and Electrical Resistivity Tomography (ERT) surveys, allowing more precise topographic correction and interpretation of geophysical data along the investigated profiles.

Previous morphotectonic and paleoseismological analyses and geophysical investigations [Patricelli et al., 2024; Rizzo et al., 2024] already suggested the presence of shallow structural features within the SE-verging Budoia-Aviano fault system, including a north-directed back-thrust component and secondary fault strands detected by ERT and GPR profiles.

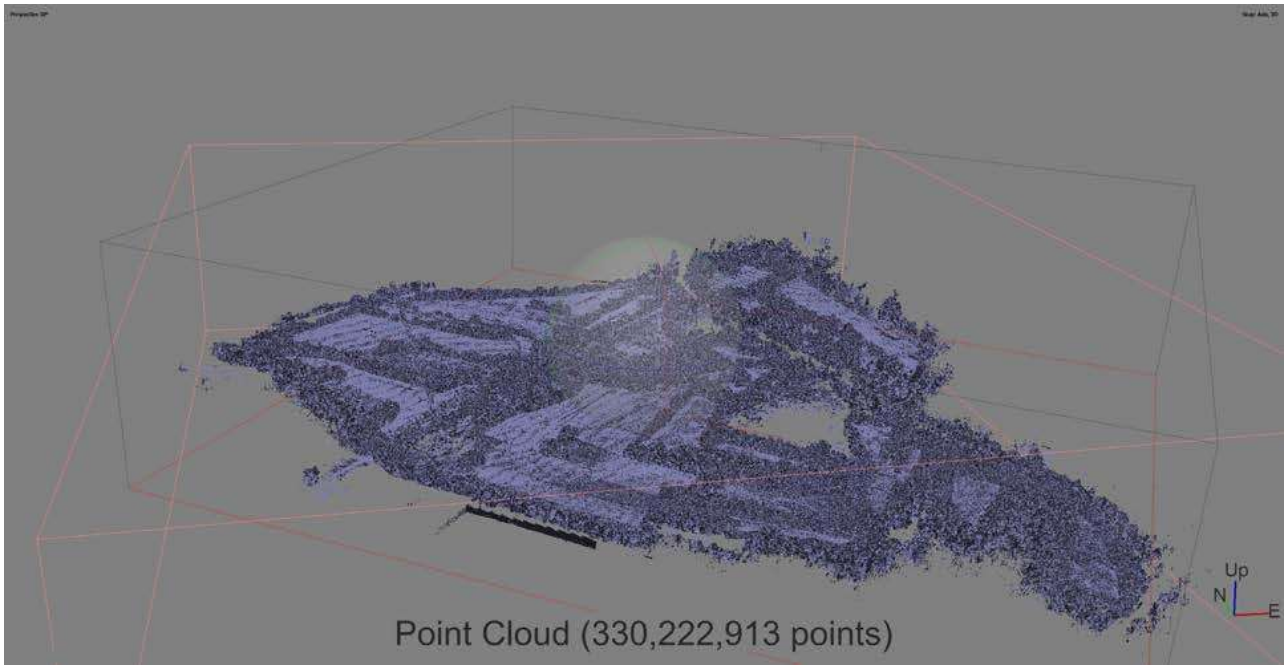

Figure 5 Unified point cloud generated automatically in GeoSLAM Connect by merging the four individual scans acquired along the Budoia–Aviano Thrust (BA). The common RTK Ground Control Points ensured accurate spatial alignment among the sectors, resulting in a seamless dataset containing more than 330 million points. This integrated point cloud represents the basis for subsequent DSM generation and morphotectonic analysis.

Building on this framework, several topographic profiles were extracted from high-resolution DSMs (Figures 6 and 7), including those generated through SLAM-based method (Figure 6), across the cultivated areas to detect subtle slope breaks and elevation variations potentially associated with active deformation. The SLAM-derived DSM proved particularly effective in highlighting minor morphological anomalies that may be related either to shallow tectonic deformation or to depositional processes, such as those shaping the alluvial fan surfaces. These newly identified features highlight additional sectors that warrant detailed investigation.

In the example shown in Figure 8, the high-resolution A-A′ DSM profile reveals a distinct slope break, transitioning from a gently southeast-dipping surface to a nearly flat area. This feature is also recognisable in the DSM derived from the regional LiDAR point cloud (LAZ format) of Friuli Venezia Giulia, whereas the DSM generated with Agisoft Metashape achieved a spatial resolution of 20.6 cm/pixel (Figure 7).

Although the main slope break at approximately 125 m along the transect could coincide with the distal portion of the late Pleistocene–Holocene Artugna alluvial fan, which has been eroded by Holocene and present-day alluvial deposits, further irregularities in the topographic profile are also observed in the southeastern portion of the transect (Figure 8). There, the upward-convex topography and minor slope breaks may indicate the presence of very shallow deformation structures, likely related to minor faulting or folding within the Budoia–Aviano Thrust system (Figure 8). The latter represents an example of surface morphology that can be further investigated through high-resolution ERT and GPR surveys.

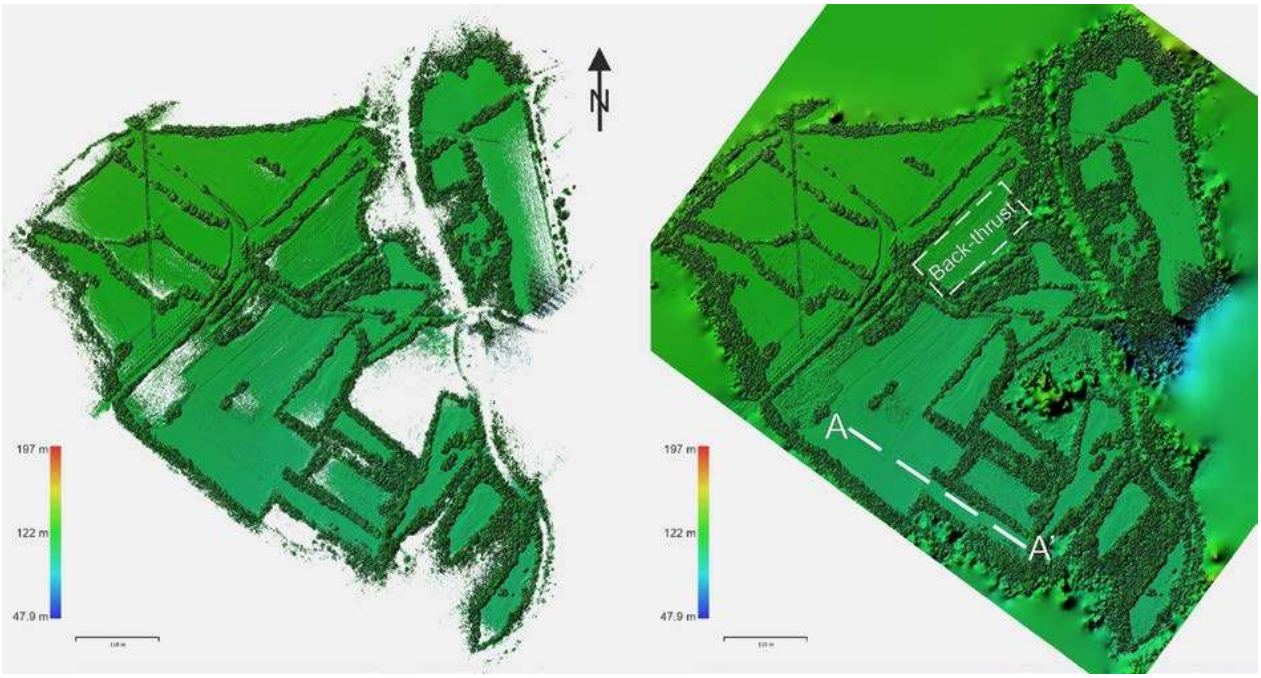

Figure 6 High-resolution Digital Surface Model (DSM) generated from the unified GeoSLAM point cloud and processed in Agisoft Metashape. The DSM, visualised at 2.7 cm/pixel resolution with an elevation colour scale ranging from 47.0 m to 197 m a.s.l., shows a slightly wider elevation range than Figure 7 due to interpolation effects. It highlights subtle topographic variations along the Budoia–Aviano Thrust area. The green–blue colour gradient enhances the morphological expression of the fault scarp and adjacent terraces. The left panel shows the DSM without interpolation, preserving the original no-data gaps, whereas the right panel displays the same model after interpolation to fill these areas.

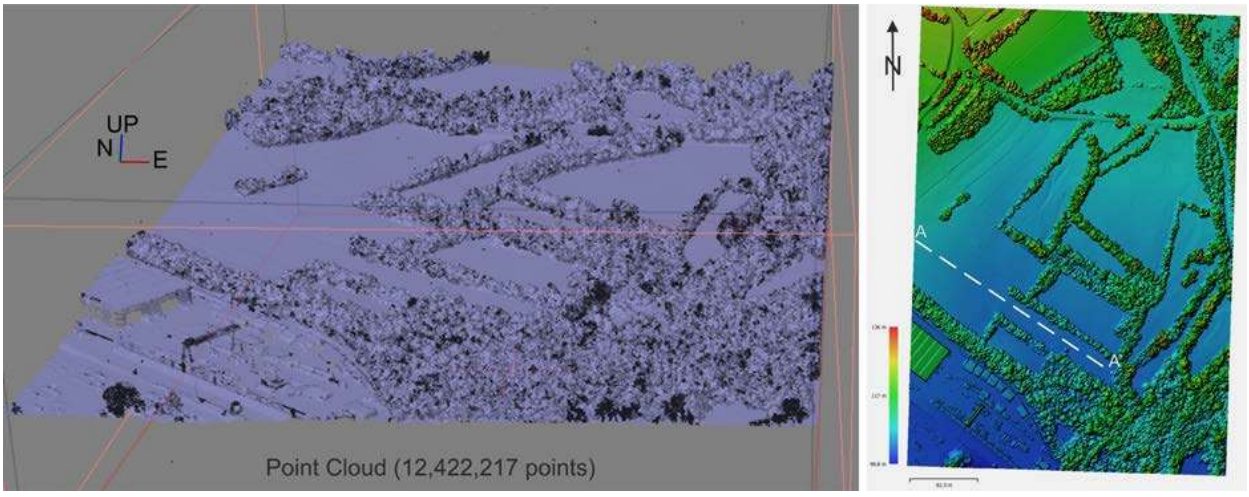

Figure 7 Left panel: Point cloud from the LiDAR dataset of Friuli Venezia Giulia. Right panel: Derived high-resolution Digital Surface Model (DSM; 20.6 cm/pixel). The elevation colour scale, ranging from 98.8 m to 136 m a.s.l., highlights subtle topographic variations along the Budoia-Aviano Thrust area.

Discussion and conclusions

The GeoSLAM-based handheld LiDAR approach proved to be a reliable and efficient method for large-area 3D surveys in restricted or operationally complex environments where UAV flights are not permitted. The technique produced high-resolution point clouds and detailed Digital Surface Models capable of capturing subtle morphological features with centimetric accuracy, which in this area can be further studied to highlight possible morphotectonic structures. Although it provides slightly lower absolute precision compared to static terrestrial or airborne laser scanning, the method ensures rapid, autonomous, and safe data acquisition across wide sectors, even in vegetated or uneven terrain.
In our case, it reproduces the same overall morphology as the FVG LiDAR survey, with slightly higher detail, as shown in Figure 8. Overall, this workflow demonstrates that mobile LiDAR technology represents a valuable and versatile tool for active tectonic studies, particularly valuable in areas affected by flight restrictions or where UAV-based photogrammetry cannot be employed, such as in correspondence of the Budoia–Aviano Thrust in the Eastern Southern Alps.

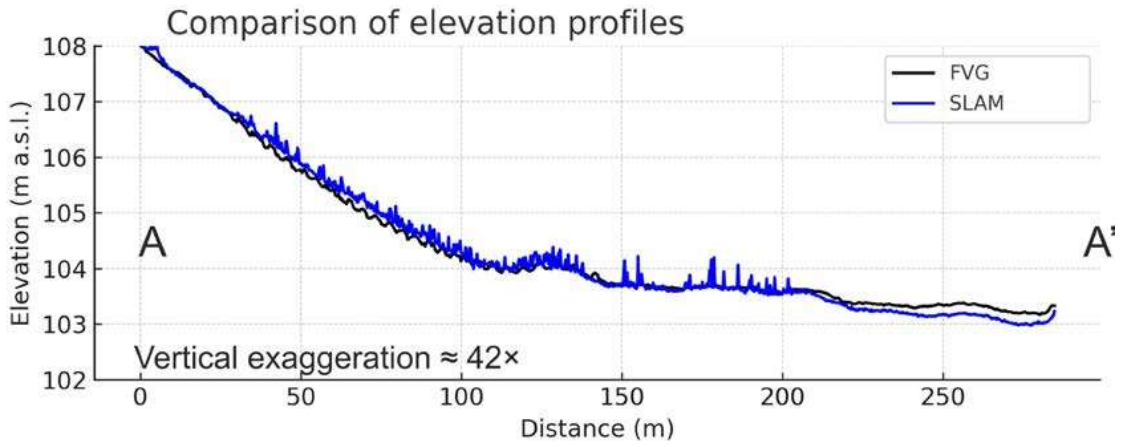

Figure 8 Comparison between two DSM-derived topographic profiles from the Budoia-Aviano Thrust area (LiDAR FVG in black; SLAM-based DSM in blue), showing a gentle slope break near 150 m along the transect. Vertical exaggeration ≈ ×42. The location of topographic transect A-A′ is shown in Figures 6 and 7.

References

Areggi, G., Pezzo, G., Merryman Boncori, J.P., Anderlin, L., Rossi, G., Serpelloni, E., Zuliani, D., and Bonini, L., (2023). *Present-day surface deformation in North-East Italy using InSAR and GNSS data*. Remote Sensing, 15(1704). https://doi.org/10.3390/rs15061704

Devoti, R., Esposito, A., Pietrantonio, G., Pisani, A., and Riguzzi,F. (2011). *Evidence of large-scale deformation patterns from GPS data in the Italian subduction boundary*. Earth and Planetary Science Letters, 311, 230-241. https://doi.org/10.1016/j.epsl.2011.09.034

Galadini, F., Poli, M.E., and Zanferrari, A., (2005). *Seismogenic sources potentially responsible for earthquakes with M > 6 in eastern Southern Alps (Thiene–Udine sector, NE Italy)*. Geophysical Journal International, 161, 739-762. https://doi.org/10.1111/j.1365-246X.2005.02571.x

Patricelli, G., Poli, M.E., Falcucci, E., Gori, S., Paiero, G., Rizzo, E., and Caputo, R., (2024). *First evidence of Holocene activity and surface displacement of the Budoia–Aviano Thrust System in north-eastern Italy, unravelled through the integration of geological, geophysical and*

paleoseismological analyses. EGU General Assembly Conference Abstracts, 16527.
Petrov, S., Dimitrov, S., and Ihtimanski, I., (2024). *Integrated application of geospatial technologies for digital twining of urbanized territories for microscale urban planning*. In Tenth International Conference on Remote Sensing and Geoinformation of the Environment (RSCy2024) (Vol. 13212, pp. 34-48). SPIE.
Poli, M.E., Monegato, G., Zanferrari, A., Falcucci, E., Marchesini, A., Grimaz, S., Malisan, P. and Del Pin, E., (2015). *Seismotectonic characterization of the western Carnic pre-alpine area between Caneva and Meduno (NE Italy, Friuli)*. DPC-INGV–S1 Project: Base-knowledge improvement for assessing the seismogenic potential of Italy (D6/a2.1).
Poli, M.E., Falcucci, E., Gori, S., Monegato, G., Zanferrari, A., Affatato, A., Baradello, L., Böem, G., Dal Bo, I., Del Pin, E., Forte, E., Grimaz, S., and Marchesini, A., (2021). *Paleoseismological evidence for historical ruptures along the Meduno Thrust (eastern Southern Alps, NE Italy)*. Tectonophysics, 818. https://doi.org/10.1016/j.tecto.2021.229071
Poli, M.E., Patricelli, G., Monegato, G., and Zanferrari, A., (2024). *Structural inheritances, fault segmentation and seismogenic potential at the front of the eastern Southern Alps (central Carnic Prealps, NE Italy)*. Tectonophysics, 883. https://doi.org/10.1016/j.tecto.2024.230390
Rizzo, E., Giampaolo, V., Mucchi, F., Boldrin, P., De Martino, G., Poli, M.E., Patricelli, G., Marchesini, A., and Caputo, R., (2024). *Multiscale geophysical investigation on the Budoia–Aviano Thrust System (NE Italy): first results*. GNGTS 2024 Proceedings.
Rovida, A., Locati, M., Camassi, R., Lolli, B., Gasperini, P., and Antonucci, A., (2022). *Catalogo Parametrico dei Terremoti Italiani (CPTI15), versione 4.0*. Istituto Nazionale di Geofisica e Vulcanologia (INGV). https://doi.org/10.13127/CPTI/CPTI15.4
Serpelloni, E., Vannucci, G., Anderlini, L., and Bennett, R.A., (2016). *Kinematics, seismotectonics and seismic potential of the eastern sector of the European Alps from GPS and seismic deformation data*. Tectonophysics, 688, 157–181. https://doi.org/10.1016/j.tecto.2016.09.026
Urban, R., Štroner, M., Braun, J., Suk, T., Kovanič, Ľ., and Blistan, P. (2024). *Determination of accuracy and usability of a SLAM scanner GeoSLAM ZEB Horizon: A bridge structure case study*. Applied Sciences, 14(12), 5258. https://doi.org/10.3390/app14125258

Sitography

[1] https://www.d-flight.it/new_portal/
[2] https://www.ingv.it/monitoraggio-e-infrastrutture/sorveglianza/servizio-di-sorveglianza-sismica